Research Article | Vol. 10, No. 10 / 1 October 2019 / Biomedical Optics Express 5015
Biomedical Optics EXPRESS

Visual method for evaluating liver function: targeted in vivo fluorescence imaging of the asialoglycoprotein receptor

XIAOJING SONG,[1,*] SHUYOU WANG,[1] CHONG ZHAO,[2] WEIBO ZHANG,[1] GUANGJUN WANG,[1] AND SHUYONG JIA[1]

[1]*Department of Biomedical Engineering, Institute of Acupuncture & Moxibustion, China Academy of Chinese Medical Sciences, Beijing, 100700, China*
[2]*Beijing Hapten and Protein Biomedical Institute, Beijing, 102206, China*
[*]*xts2010@163.com*

Abstract: The visual evaluation of liver function (LF) has always been a hot topic in research on liver diseases. In vivo fluorescence imaging (IVFI) of the Cy5.5-galactosylated polylysine (Cy5.5-GP) probe targeting asialoglycoprotein receptor (ASGPR), for evaluating LF in chronic alcoholic liver injury (cALI) mice was investigated in this study. The decrease of fluorescence signals in the livers showed a biological relationship with the liver ASGPR expression, histology, and serum marker levels of LF in cALI mice. The targeted IVFI of ASGPR as a novel method can intuitively and noninvasively display the characteristics of liver's ASGPR level to provide a reference for evaluating LF.

1. Introduction

In clinical and basic research, evaluating liver function (LF) is crucial for determining the diagnosis, guiding treatment and determining the therapeutic effect in liver disease. Sakka, a German scholar [1], divided methods for evaluating LF into static and dynamic tests. Static tests were the earliest and are the most common methods for evaluating LF and include routine blood biochemical tests, such as bilirubin, coagulation factor, albumin, serum creatinine and serum sodium analyses. However, the degree of hepatocyte injury and residual LF cannot be quantified in real time. Dynamic detection methods include clearance and breathing tests, which can effectively evaluate the metabolic function of the liver and have the advantage of quantitatively evaluating LF in real time. However, these tests do not allow the qualitative or localized diagnosis of liver lesions due to the influence of the basal metabolic rate, smoking and other factors. With the development of imaging technology, more visual LF evaluation methods have been developed. Currently, the commonly used imaging techniques for evaluating LF include ultrasound, computed tomography (CT), magnetic resonance imaging (MRI) and positron emission tomography (PET). Ultrasonography can aid in the diagnosis of space-occupying liver lesions, but its sensitivity for detecting relatively small lesions of 1-5 cm in diameter is less than 50%, and it exhibits low diagnostic accuracy and no qualitative LF assessment capacity [2,3]. CT has certain advantages in the diagnosis of parenchymal liver lesions and is considered the first choice among noninvasive diagnostic methods because it can best reflect pathomorphological manifestations in the liver. However, the accurate qualitative diagnosis and evaluation of LF cannot be carried out [4,5]. Because of its high resolution, MRI can be used for the qualitative diagnosis and assessment of LF. However, compared with optical imaging, its sensitivity is relatively low. Moreover, MRI equipment is expensive, and its cost is relatively high when used for animal studies [6,7]. Digital subtraction angiography is primarily an auxiliary examination method for hepatic artery embolism [8]. PET has relatively high clinical value in tumour monitoring and differential diagnosis. However, its diagnostic sensitivity for liver injury due to

#370449 https://doi.org/10.1364/BOE.10.005015
Journal © 2019 Received 20 Jun 2019; revised 28 Aug 2019; accepted 1 Sep 2019; published 9 Sep 2019

Biomedical Optics EXPRESS

other causes is relatively low [9]. The above imaging methods are primarily advantageous for the diagnosis of hepatic vascular lesions and space-occupying lesions, but deficiencies in the dynamic visualization and monitoring of LF for other liver diseases still exist, especially in terms of localization, diagnosis and quantitative evaluation at the cellular and molecular levels. Using molecular imaging technology to develop novel LF detection methods has become an important direction in the visual evaluation of LF.

Recently, researchers applied the scanning specificity of single-photon emission tomography (SPECT) technology with the asialoglycoprotein receptor (ASGPR) ligand ^{99m}TcGSA to target hepatocytes and dynamically visualize the function of hepatocytes at the molecular level with the aim of evaluating liver reserve function [10]. However, because SPECT uses radioactive tracers and photonic imaging principles, it still has deficiencies in terms of biosafety and image quality. In addition, its cost is high for animal studies. IVFI is a novel optical imaging technology developed over recent years. It takes advantage of the optical radiation of bioluminescence and fluorescence at 500-950 nm to display and quantify the site and intensity of luminescence for the in vivo diagnostic imaging of animals. This technique has the advantages of non-invasiveness, high sensitivity, good specificity, ease of operation, non-radioactivity and relatively low cost. At the same time, it has great advantages for real-time, dynamic evaluations [11,12]. Therefore, IVFI technology is generally more suitable than PET imaging for animal studies in LF evaluation.

However, to the best of our knowledge, the successful application of fluorescent probe for monitoring LF has not yet been reported. In this study, the fluorescent probe, Cy5.5- conjugated galactosylated polylysine (Cy5.5-GP), which targets hepatocyte ASGPR was used to observe the IVFI characteristics of liver tissue in healthy mice and mice with chronic alcoholic liver injury (cALI) for the first time. We investigated whether the novel method of IVFI of Cy5.5-GP targeting ASGPR can be used to assess LF in physiological and pathological conditions.

2. Material and methods

2.1. Animals and groups

In all, the 90 healthy adult male Kunming mice with an average age of 3 weeks, and weight of 20-22 g were used in this study. All animals were provided by the Biotechnology Co., Ltd. (SCXK (Beijing) 2016-0002). They were treated in accordance with international standards for the care and use of laboratory animals, and the entire experiment was performed in accordance with the protocol approved by the Animal Ethics Committee of the Institute of Acupuncture and Moxibustion at the China Academy of Chinese Medical Science (No.20140013). The animals were randomly divided into six groups: control group I (CG I), Cy5.5-GP was injected into the tail vein of 20 healthy mice after 4 weeks of normal care; control group II (CG II), after 4 weeks of normal care, a sufficient amount of galactosylated polylysine was injected into the tail vein of 20 healthy mice, and then, Cy5.5-GP was injected; control group III (CG III), Cy5.5 was injected into the tail vein of 5 healthy mice after 4 weeks of normal care; cALI group I (cALIG I), after successful development of the ALI model, Cy5.5-GP was injected into the tail vein of 20 mice; cALI group II (cALIG II), after successful development of the cALI model, a sufficient amount of galactosylated polylysine was injected into the tail vein of 20 mice to block ASGPR, and then, Cy5.5-GP was injected; and cALI group III (cALIG III), after successful development of the ALI model, Cy5.5 was injected into the tail vein of 5 mice.

2.2. Construction of the cALI model

After 12 h of fasting, the Kunming mice were subjected to gavage with 50% ethanol (15 mL/kg/bw) daily for 4 weeks. Criteria for successful identification of the model were as follows: (1) blood biochemical index levels, including serum alanine aminotransferase (ALT) and aspartate aminotransferase (AST) levels, were significantly increased; (2) the liver was dimmer in colour

Biomedical Optics EXPRESS

and harder in texture than normal livers and exhibited petechiae, with some surfaces showing slightly increased roughness, while the relative weight of the liver increased; (3) examination of liver tissue by a light microscopy, after haematoxylin and eosin (H&E) staining showed the disappearance of hepatic cord structures, hepatocyte enlargement, cytoplasmic rarefaction, a large number of fat droplets in hepatocytes (with the nucleus pushed to the edge), and signs of necrosis and disintegration in some hepatocytes. The appearance of the above characteristics indicated successful construction of the model [13].

2.3. Tail vein injection

After full anaesthetization by the inhalation of isoflurane gas, the CG I and cALIG I mice were injected via the tail vein with 300 μL Cy5.5-GP solution (0.005 μg/μL, 0.01 mL/g) (Beijing Hapten and Protein Biomedical Institute, China). The CG II and cALIG II mice were injected with 200 μL galactosylated polylysine (0.05 mg/kg) (Beijing Hapten and Protein Biomedical Institute, China) via the tail vein to bind ASGPR, and were then injected with 300 μL Cy5.5-GP solution via the tail vein 45 min later. The CG III and cALI III mice were injected with 300 μL Cy5.5 (0.001 μg/μL, 0.01 mL/g) (Beijing Hapten and Protein Biomedical Institute, China) via the tail vein.

2.4. IVFI

After intravenous injection via the tail vein, the mice were placed flat in a prone position in the dark recording chamber of an FX PRO multi-modal in vivo imaging system (Carestream Health Inc., USA). The instrumental parameters were set as follows: excitation wavelength, 630 nm; emission wavelength, 700 nm; exposure time, 10 seconds. Images were acquired immediately after the Cy5.5-GP or Cy5.5 solution was injected via tail vein; then images were collected at 10, 30, 60, 90, 120 and 150 min after injection. Systematic and local visual analysis after probe injection was performed by IVFI. The fluorescence signal characteristics of the liver were compared between the ASGPR-blocked and non-ASGPR-blocked groups, and healthy and cALI animals, to determine whether the probe specifically targeted the liver. Anesthesia was maintained with inhalation of isoflurane gas throughout the operation. Two mice of each group were randomly sacrificed by exsanguination at 60 min after the Cy5.5-GP injection. The entire liver lobe was immediately removed by laparotomy and placed in the dark recording chamber to acquire fluorescence images of the liver lobe using the same instrumental parameters as those described above. The fluorescence signal intensity (FI) and fluorescence aggregation area (FA) in the liver at each time point were analysed using the Carestream molecular imaging software (Carestream Health Inc., USA).

2.5. Serum markers of LF

At 24 h after Cy5.5-GP injection, 1.5 mL blood was collected from the mouse heart. After 1 h, it was centrifuged for 5000 rpm at 4 °C for 10 min in a high-speed centrifuge to obtain the serum. Total levels of bile acid (TBA) and the ALT, AST, and gamma-glutamyl transferase (GGT) were detected using an Accute TBA-40FR automatic biochemical analyser (Toshiba Zhuzhou Sanguang Medical Co., Ltd., Japan).

2.6. Western blot and ELISA

After blood sampling, the liver tissues were cut quickly. The liver tissue (50 mg) was added to cold RIPA buffer (500 μL) and homogenized, the homogenate was centrifuged for 10000 rpm at 4 °C for 20 min in a high-speed centrifuge to obtain the supernatant. The total protein concentration in the supernatant was quantified by Bradford Assays (Thermo Pierce Rapid Gold BCA Protein Assay Kit, Thermo Scientific, USA). The supernatant mixed with a certain proportion of 5× and 1× SDS-PAGE loading buffer (Solarbio, China) were boiled at 95°C for 10 min. Equal amounts

Biomedical Optics EXPRESS

of protein (50 μg/20 μL) was separated by 10% SDS-PAGE (SDS-PAGE Gel Kit, Solarbio Life Sciences, China). Proteins were electrophoretically transferred to polyvinylidene difluoride membranes (Bio-Rad, Rich-mond, USA) which were then blotted with ASGPR1 antibody [N1C3] (GeneTeX International Corporation, USA) diluted 1:3000. The secondary antibody (IRDye 800CW, LI-COR Biosciences, USA) was used to detect the primary antibody. Anti-alpha tubulin antibody (Loading control ab89984, Abcam, England) and secondary antibody (IRDye 680LT, LI-COR Biosciences, USA) were used as references. Band signals were detected using an infrared laser scan imaging system (LI-COR Odyssey, USA) and analysed using Odyssey Classic Software (LI-COR, USA). In addition, the ASGPR content was determined using an ASGPR ELISA kit (Shanghai Jianglai Industrial Limited By Share Ltd., Shanghai, China) following the manufacturer's protocol. A STAT FAX 2100 automatic microplate reader (Awareness Technology Inc., USA) was used for detection and analysis.

2.7. H&E staining of liver tissue

A piece of liver tissue ($1 \times 0.5 \times 0.2$ cm) was collected 5 mm from the edge of the liver in ten randomly selected mice from CG I and cALIG I. After the tissue was fixed with 10% formalin, and embedded in paraffin, sections were prepared at a thickness of 6μm, followed by conventional H&E staining. The structural and pathological changes of the liver tissue and cells were observed by an optical microscopy.

2.8. Statistical analysis

SPSS19.0 statistical software was used for statistical analysis. The mean FI and FA in each group were calculated at each time point. The mean levels of ASGPR, ALT, AST, GGT, and TBA were calculated for each group. One-way ANOVA was used to compare differences in the same index among the groups, and the LSD test for two-group comparisons was performed to determine significant differences between groups. The data are expressed as the mean ± SD, with $P < 0.05$ indicating statistical significance.

3. Results and discussion

3.1. IVFI characteristics of the liver in mice

At each time point, the images of IVFI visually displayed the obvious differences in the fluorescence probe distributions among the groups. After the Cy5.5-GP injection, slow fluorescence aggregation was observed in the liver area of mice in CG I and cALI I. In the CG I, from 10-30 min after injection, the FI and FA of the liver area gradually increased; from 30-60 min after injection, the FI reached the highest level, and the FA was the largest; from 30-90 min after injection, the fluorescence signals were stable; at 120 min after injection, the FI in the liver area began to attenuate, and the FA decreased; at 150 min after injection, the fluorescence signal in the liver area continuously attenuated (Fig. 1(A)). However, in the CG II, after blocking ASGPR in the liver via the intravenous injection of a sufficient amount of galactosylated polylysine, no fluorescence signal aggregation was observed in the liver in total 150 min of observation (Fig. 1(B)). At the same threshold, the fluorescence signal of image display in healthy mouse of CG I was stronger than that in cALI I. Then there is the problem of spontaneous fluorescence singles of animal skin, the mouth of mouse showed strong fluorescence signal too in Fig. 1(A).

In the cALIG I, fluorescence signal aggregation did not occur within 10 min after fluorescence probe injection. At 30 min after probe injection, fluorescence signal aggregation appeared in the liver region. However, the FI was weaker than that in CG I, and the FA was smaller. At 60 min after injection, the fluorescence signal aggregation in the liver reached the highest level. At 90 min after injection, the FI in the liver began to attenuate, and the FA decreased; at 150 min after injection, the fluorescence signal in the liver area reduced to half of the maximum. At the

Biomedical Optics EXPRESS

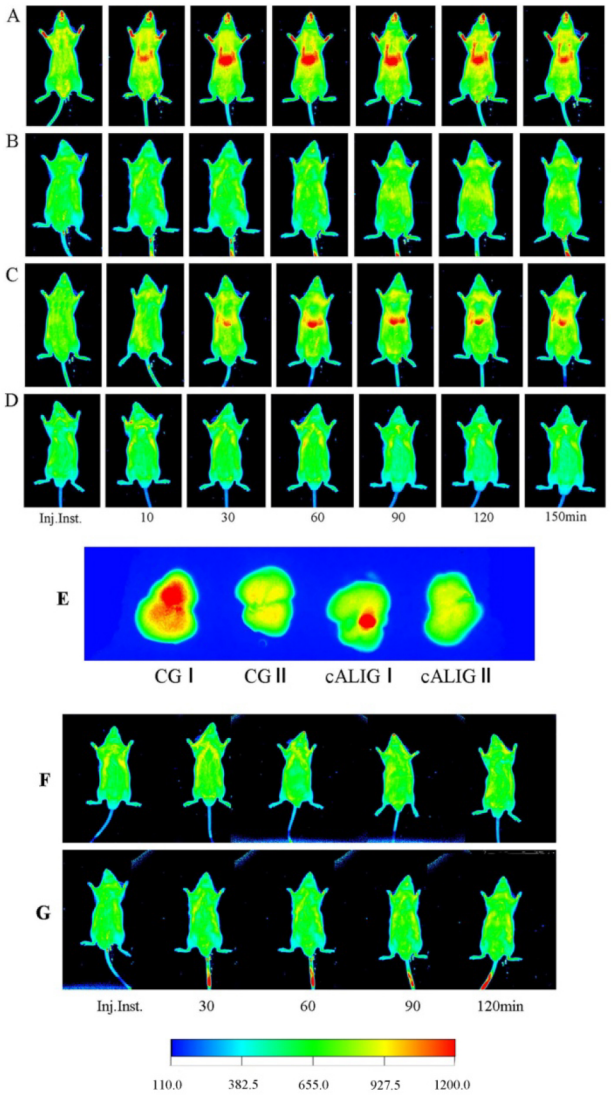

Fig. 1. Targeted visualization of ASGPR by IVFI with Cy5.5-GP. On IVFI, the red area in the middle of the mouse abdomen indicates Cy5.5-GP binding with hepatocyte ASGPR. Inj. inst.: Immediately after Cy5.5-GP injection. A: Cy5.5-GP IVFI, CG I ($n = 10$). After Cy5.5-GP injection, slow aggregation of fluorescence in the liver was observed; from 10-30 min, the FI gradually increased; from 30-60 min, the FI reached the highest level, and the FA was the largest; from 60-90 min, the FI and FA were stable; at 120 min, the FI was slightly decreased, and the FA was decreased; at 150 min, the FI was significantly attenuated. B: Cy5.5-GP IVFI, CG II ($n = 10$). There was no fluorescence signal aggregation in the liver at any point. C: Cy5.5-GP IVFI, cALIG I ($n = 10$). From 30-150 min, the fluorescence distribution characteristics in the liver were similar to that in CG I; however, the FA was significantly lower than that in CG I. D: Cy5.5-GP IVFI, CG II ($n = 10$). The results are consistent with those observed in CG II. E: IVFI of the liver lobe at 60 min after Cy5.5-GP injection; $n = 2$ animals in each group. The FI was highest in CG I, followed by cALIG I, CG II and cALIG II. F: Cy5.5 IVFI, CG III ($n = 5$). G: Cy5.5 IVFI, cALIG III ($n = 5$). There was no fluorescence signal aggregation in the liver at any time point in the latter two groups. The color index was intensity scale.

Biomedical Optics EXPRESS

same time point, the FI and FA of the liver area in the cALIG I were smaller than those in the CG I (Fig. 1(A, C)). In the cALIG II, as in CG II, no specific fluorescence signal aggregation was observed in the liver during the observation period (Fig. 1(D)).

In addition, liver lobes were obtained from two mice in each group at 60 min for individual imaging. The images showed that the FI of the liver tissue was highest in CG I, followed by cALIG I, CG II, and cALIG II (Fig. 1(E)). In the CG III and cALIG III, no specific fluorescence signal aggregation was observed in the mice after Cy5.5 injection during observation period (Fig. 1(F, G)). These results showed that relatively good specificity of Cy5.5-GP for binding liver's ASGPR and its potential to be used in ASGPR-targeted fluorescence imaging. In Fig. 1(G), the tail was fluorescent at 30, 60, 90, 120 min after injection since the tail skin of this mouse was stained with dye in the process of experiment.

3.2. Quantification of fluorescence imaging signals

At 10, 30, 60, 90, and 120 min after Cy5.5-GP injection, the FI of the liver area in CG I was significantly higher than that in cALIG I, $P < 0.01$ (Fig. 2(A)). From 10 min to 150 min after Cy5.5-GP injection, the FA of the liver area in CG I was always significantly larger than that in cALIG I, $P < 0.01$ (Fig. 2(B)). The results directly displayed the dynamic process of the Cy5.5-GP probe binding ASGPR. It indicated that the Cy5.5-GP probe exhibited stable and efficient binding with ASGPR in vivo. The largest difference of FI and FA were both found at 60 min after Cy5.5-GP injection between the two groups, suggesting that the ASGPR level of the liver in healthy mice was much higher than that in the cALI mice. Thus, at 60 min after Cy5.5-GP injection, the targeted IVFI of ASGPR could be used for intuitive demonstration of ASGPR level changes in the liver.

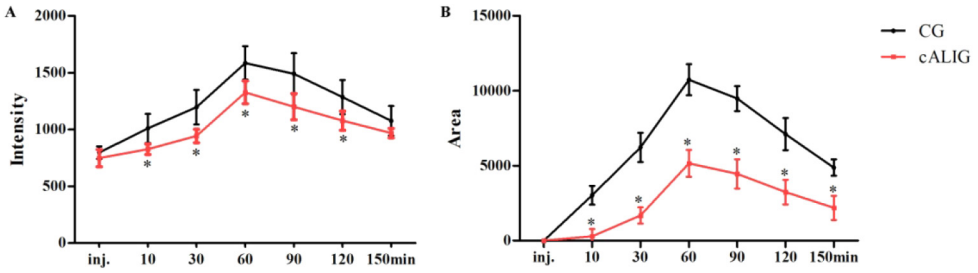

Fig. 2. Quantification of Cy5.5-GP data between CG I and cALIG I. A: Liver Cy5.5-GP FI over time. B: Liver Cy5.5-GP FA over time. (*$P < 0.01$ vs CG, LSD two-group comparison test; $n = 10$ animals in each group). inj.: Immediately after Cy5.5-GP injection. The data are shown as the mean ± SD.

3.3. ASGPR expression in the liver

Western blotting indicated that ASGPR expression in the liver in the cALI groups (0.87 ± 0.3%) was significantly lower than that in the control groups (1.83 ± 0.5%), while tubulin expression in the liver in the two groups was equivalent (Fig. 3(A, B)). ELISA showed that the ASGPR content of the liver in the control groups was significantly lower (219.03 ± 16.34 ng/μL) than that in the cALI groups (190.08 ± 19.46 ng/μL), $P < 0.05$ (Fig. 3(C)). ASGPR is a protein expressed on the membrane surface of normal and regenerated hepatocytes. In liver disease, such as hepatitis, alcoholic liver disease, cirrhosis and liver cancer, hepatocytes become necrotic, ASGPR activity is impaired, and the ASGPR level significantly decreases [14,15]. The results indicated the normal hepatocytes reduced in cALI mice. In addition, ASGPR's quantity and function are positively correlated with the function of liver cells [16]. Detection of ASGPR level is a sensitive method for assessing liver reserve function [17,18]. The imaging characteristics of a weak FI and

Biomedical Optics EXPRESS

small FA in the liver of cALI mice were consistent with the low ASGPR expression in the liver, it suggested the changes of FI and FA in the liver area can be used to display the ASGPR level to assess liver reserve function in a dynamic and non-invasive manner.

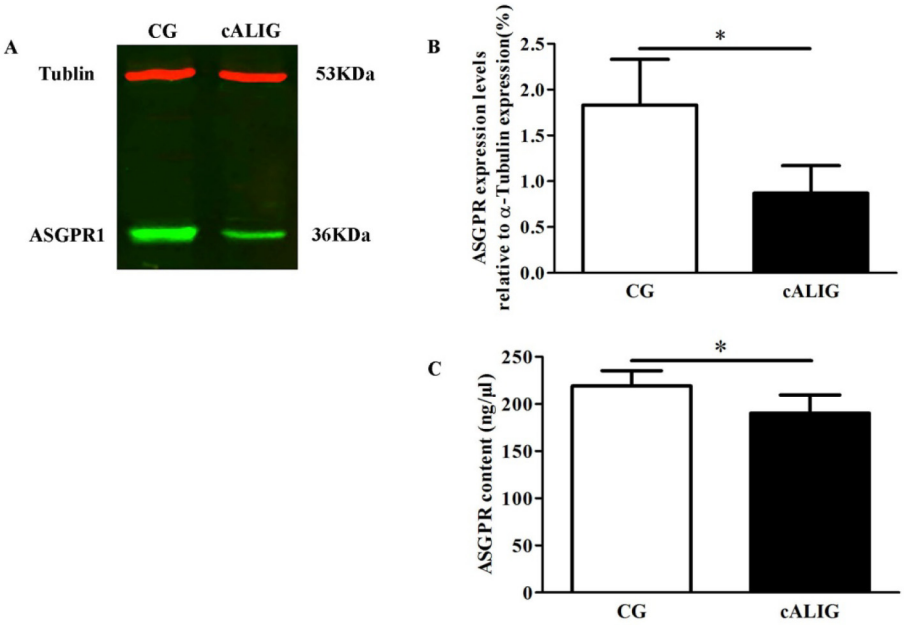

Fig. 3. ASGPR expression in the liver tissue of healthy mice (CG I) and cALI mice (cALIG I). A: ASGPR expression in hepatocytes determined by Western blot analysis. ASGPR and tubulin expression in CG (lane 1) and cALIG (lane 2); $n = 10$ animals in each group. B: Densitometric analysis of the Western blot results of ASGPR expression based on tubulin expression; $n = 10$ animals in each group. C: Densitometric analysis of ASGPR expression by ELISA; $n = 10$ animals in each group. (*$P < 0.05$ vs CG; LSD two-group comparison test). The data are shown as the mean ± SD.

3.4. Liver histology and LF serum marker levels

Long-term alcohol intake can lead to pathological changes of liver tissue and severe liver function damage, including inflammation, steatosis and even fibrosis [19-22]. In the CG I, the hepatic lobule structure was intact and clear. The hepatocytes were polygonal in shape, uniform in size, and arranged in cords that radiated around the central vein, and irregular hepatic sinusoids were present between the hepatic cords, which were regularly distributed. A few red blood cells were observed in the sinus (Fig. 4(A)). In the cALIG I, destruction of the hepatic lobule structure and disordered arrangement of the hepatocyte cords were observed. Hepatocytes around the vein were enlarged with slightly stained cytoplasm, leading to focal necrosis. Vacuoles of different sizes were found in hepatocytes distant from the central vein. Hepatocyte steatosis accompanied by inflammatory cell infiltration was observed (Fig. 4(B)). In addition, the ALT, AST and GGT levels were significantly higher in cALIG I than in CG I ($P < 0.05$) (Fig. 4(C-E)). The TBA content was also increased; however, the difference between the two groups was not significant (Fig. 4(F)). The abnormal changes of liver histomorphology and serum markers of LF in cALI mice suggested liver function injury appeared. Therefore, it implied that the characteristics of IVFI of Cy5.5-GP targeting ASGPR can display the differences of liver function between healthy and cALI mice, and provide a reference for assessing liver function.

Biomedical Optics EXPRESS

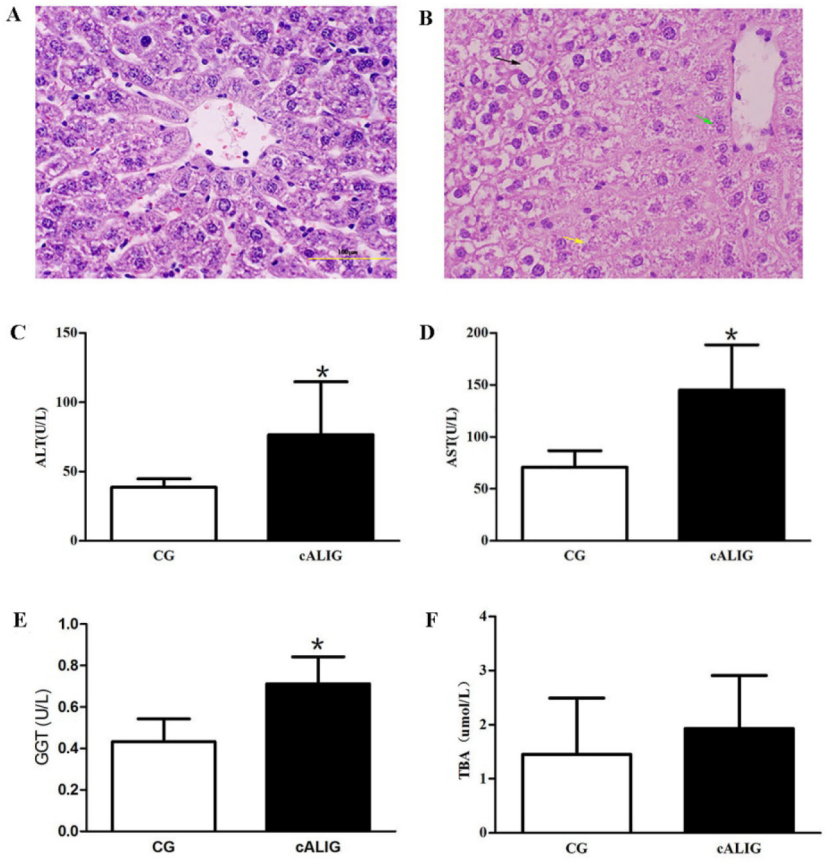

Fig. 4. Comparison of liver histology and serum marker levels. A and B: H&E staining of liver tissue (10×); scale bar: 100 μm, A was CG I, B was cALIG I; $n = 10$ animals in each group. The black arrow indicates steatotic hepatocytes, the yellow arrow indicates necrotic hepatocytes, and the green arrow indicates swollen and distended hepatocytes. C: Comparison of the ALT level between CG I and cALIG I; $n = 10$ animals in each group. D: Comparison of the AST level between the two groups; $n = 10$ animals in each group. E: Comparison of the GGT level between the two groups; $n = 10$ animals in each group. F: Comparison of the TBA level between the two groups; $n = 10$ animals in each group. (*$P < 0.05$ vs CG; LSD two-group comparison test). The data are shown as the mean ± SD.

4. Conclusion

Due to the advantages of high sensitivity, non-invasiveness, real-time and dynamic imaging [23-25], in this study, the IVFI of Cy5.5-GP targeting ASGPR was established, and used to observe the dynamic imaging characteristics of an ASGPR-targeting marker in the liver of healthy and cALI mice for the first time. After Cy5.5-GP injection, *in vivo* and *in vitro* the specific fluorescence signals aggregation of the liver appeared in the healthy and cALI mice, and the FI and FA were significantly higher in liver area of the healthy mice than that of cALIG mice. By blocking ASGPR, the specific aggregation of fluorescence probe can be prevented. And the imaging characteristics of weak FI and small FA of liver area were consistent with the decline of ASGPR level, increase of ALT, AST, GGT and TBA levels, and hepatocyte steatosis, inflammatory cell infiltration and focal necrosis in liver tissue in cALI mice. It indicated the changes of FI and FA in the liver region can be used to display the ASGPR level in an intuitive

Biomedical Optics EXPRESS

and non-invasive manner. Therefore, it implied that the characteristics of IVFI of Cy5.5-GP targeting ASGPR can display the difference of liver reserve function between healthy and cALI mice, and provide a reference for assessing liver function in physiological and pathological condition. Compared with ultrasound, CT and MRI, this technique has the advantages of specific localization, quantitative evaluation at the level of hepatic receptors and cells, and early and sensitive determination of the degree of hepatocyte injury, and it can be used to assess residual LF. Compared with SPECT, this imaging method is more environmentally friendly and economical for animal studies. Therefore, IVFI of Cy5.5-GP targeting ASGPR, this molecular imaging technique has practical application in the basic research of drug research and development, liver pathology and toxicology assessments, liver transplantation monitoring, and liver tumour diagnosis and treatment in animal experimental. Of course, this method still requires improvement in future research.

Funding

National Natural Science Foundation of China (81704175).

Acknowledgements

We acknowledge support from China Research Foundation and Institute of Acupuncture & Moxibustion, China Academy of Chinese Medical Sciences. We thank American Journal Expert (AJE) for providing English editing.

Disclosures

The authors declare that there are no conflicts of interest related to this article.

References

1. S. G. Sakka, "Assessing liver function," Curr. Opin. Crit. Care. **13**(2), 207–214 (2007).
2. S. R. Wilson and P. N. Burns, "An algorithm for the diagnosis of focal liver masses using microbubble contrast-enhanced pulse-inversion sonography," AJR, Am. J. Roentgenol. **186**(5), 1401–1412 (2006).
3. H. Y. Zhai, P. Liang, J. Yu, F. Cao, M. Kuang, F. Y. Liu, F. Y. Liu, and X. Y. Zhu, "Comparison of Sonazoid and Sonovue in the Diagnosis of Focal Liver Lesions: A Preliminary Study," J. Ultrasound. Med. **38**(9), 2417–2425 (2019).
4. S. Amano, M. Ebara, T. Yajima, H. Fukuda, M. Yoshikawa, N. Sugiura, K. Kato, F. Kondo, T. Matsumoto, and H. Saisho, "Assessment of cancer cell differentiation in small hepatocellular carcinoma by computed tomography and magnetic resonance imaging," J. Gastroenterol. Hepatol. **18**(3), 273–279 (2003).
5. R. K. Do, A. McErlean, C. S. Ang, R. P. DeMatteo, and G. K. Abou-Alfa, "CT and MRI of primary and metastatic fibrolamellar carcinoma: a case series of 37 patients," Br. J. Radiol. **87**(1040), 20140024 (2014).
6. T. Hennedige and S. K. Venkatesh, "Imaging of hepatocellular carcinoma: diagnosis, staging and treatment monitoring," Cancer Imaging. **12**(3), 530–547 (2012).
7. L. Petitclerc, G. Sebastiani, G. Gilbert, G. Cloutier, and A. Tang, "Liver fibrosis: Review of current imaging and MRI quantification techniques," J. Magn. Reson. Imaging. **45**(5), 1276–1295 (2017).
8. K. Ozaki, S. Kobayashi, O. Matsui, T. Minami, W. Koda, and T. Gabata, "Extrahepatic Arteries Originating from Hepatic Arteries: Analysis Using CT During Hepatic Arteriography and Visualization on Digital Subtraction Angiography," Cardiovasc. Intervent. Radiol. **40**(6), 822–830 (2017).
9. M. A. Khan, C. S. Combs, E. M. Brunt, V. J. Lowe, M. K. Wolverson, H. Solomon, B. T. Collins, and A. M. Di Bisceglie, "Positron emission tomography scanning in the evaluation of hepatocellular carcinoma," J. Hepatol. **32**(5), 792–797 (2000).
10. D. Zhang, Z. Guo, P. Zhang, Y. Li, X. H. Su, L. Y. You, M. Gao, C. Liu, H. Wu, and X. Z. Zhang, "Simplified quantification method for in vivo SPECT/CT imaging of asialoglycoprotein receptor with (99 m)Tc-p(VLA-co-VNI) to assess and stage hepatic fibrosis in mice," Sci. Rep. **6**(1), 25377 (2016).
11. H.W. Lee, P. G angadaran, S. Kalimuthu, and A. Byeong-Cheol, "Advances in Molecular Imaging Strategies for In Vivo Tracking of Immune Cells," BioMed Res. Int. **2016**, 1946585 (2016).
12. M. Furuya and M. Ishii, "Frontiers in live bone imaging researches. In vivo imaging of osteoblasts," Clin. Calcium. **25**(6), 823–830 (2015).
13. A. Bertola, S. Mathews, S. H. Ki, H. Wang, and B. Gao, "Mouse model of chronic and binge ethanol feeding (the NIAAA model)," Nat. Protoc. **8**(3), 627–637 (2013).

Biomedical Optics EXPRESS

14. D. Villalta, M. G. Mytilinaiou, M. Elsner, C. Hentschel, J. Cuccato, V. Somma, P. Schierack, D. Roggenbuck, and D. P. Bogdanos, "Autoantibodies to asialoglycoprotein receptor (ASGPR) in patients with autoimmune liver diseases," Clin. Chim. Acta **450**, 1–5 (2015).
15. B. L. McVicker, G. M. Thiele, D. J. Tuma, and C. A. Casey, "Hepatocyte-mediated cytotoxicity and host defense mechanisms in the alcohol-injured liver," Hepatol. Int. **8**(S2), 432–438 (2014).
16. J. Hu, J. Liu, D. Yang, M. Lu, and J. Yin, "Physiological roles of asialoglycoprotein receptors (ASGPRs) variants and recent advances in hepatic-targeted delivery of therapeutic molecules via ASGPRs," Protein Pept. Lett. **21**(10), 1025–1030 (2014).
17. Z. Ke, J. Li, J. Zhe, L. B. Liang, L. Yan, and M. Yi, "Flow cytometric analysis of asialoglycoprotein receptor expression predicts hepatic functional reserve after hepatectomy," J. Coll. Physicians. Surg. Pak. **24**(11), 820–824 (2014).
18. W. Jing, J. Li, L. Q. Tao, J. Zhe, L. B. Liang, and Z. Ke, "Prediction of asialoglycoprotein receptors by correlated liver function parameters before hepatectomy," J. Pak. Med. Assoc. **66**(Suppl 3), S56–S58 (2016).
19. M. Matsumoto, I. Cyganek, P. C. Sanghani, W. K. Cho, S. Liangpunsakul, and D. W. Crabb, "Ethanol metabolism by HeLa cells transduced with human alcohol dehydrogenase isoenzymes: control of the pathway by acetaldehyde concentration," Alcohol.: Clin. Exp. Res. **35**(1), 28–38 (2011).
20. T. Radosavljević, D. Mladenović, and D. Vucević, "The role of oxidative stress in alcoholic liver injury," Med. Pregl. **62**(11-12), 547–553 (2009).
21. D. Zhang, X.J. Song, S.Y. Li, S.Y. Wang, B.J. Chen, X.D. Bai, and L.M. Tang, "Evaluation of liver function and electroacupuncture efficacy of animals with alcoholic liver injury by the novel imaging methods," Sci. Rep. **6**(1), 30119 (2016).
22. G. Szabo, B. Saha, and T. N. Bukong, "Alcohol and HCV: implications for liver cancer," Adv. Exp. Med. Biol. **815**, 197–216 (2015).
23. V. Ntziachristos and D. Razansky, "Optical and opto-acoustic imaging," Recent Results Cancer Res. **187**, 133–150 (2013).
24. H. Y. Zhang, O. H. Aina, K. S. Lam, R. de Vere White, E. Christopher, H. Paul, P. N. Lara, X. Wang, J. A. Bassuk, and C. X. Pan, "Identification of a bladder cancer-specific ligand using a combinatorial chemistry approach," Urol. Oncol. **30**(5), 635–645 (2012).
25. W. Han, R. Zaynagetdinov, F. E. Yull, V. V. Polosukhin, L. A. Gleaves, and H. Tanjore, "Molecular imaging of folate receptor β-positive macrophages during acute lung inflammation," Am. J. Respir. Cell Mol. Biol. **53**(1), 50–59 (2015).